STRUCTURE OF DISK DOMINATED GALAXIES: II. COLOR GRADIENTS AND STELLAR POPULATION MODELS

Lauren A. MacArthur

Department of Physics & Astronomy, University of British Columbia, 6224 Agricultural Road, Vancouver, BC CANADA V6T 1Z1

STÉPHANE COURTEAU
Department of Physics, Queen's University, Kingston, ON CANADA K7L 3N6

AND

Jon A. Holtzman

Department of Astronomy, New Mexico State University, Box 30001, Department 45000, Las Cruces, NM 88003-8001 For Publication in ApJ Supplements

ABSTRACT

We investigate optical and near-IR color gradients in a sample of 172 low-inclination galaxies spanning Hubble types S0-Irr. The colors are compared to stellar population synthesis models from which luminosity-weighted average ages and metallicities are determined. We explore the effects of different underlying star formation histories and additional bursts of star formation. Our results are robust in a relative sense under the assumption that our galaxies shared a similar underlying star formation history and that no bursts involving more than $\sim 10\%$ of the galaxy mass have occurred in the past 1-2 Gyr. Because the observed gradients show radial structure, we measure "inner" and "outer" disk age and metallicity gradients. Trends in age and metallicity and their gradients are explored as a function of Hubble type, rotational velocity, total near-IR galaxy magnitude, central surface brightness, and scale length. We find strong correlations in age and metallicity with Hubble-type, rotational velocity, total magnitude, and central surface brightness in the sense that earlier-type, faster rotating, more luminous, and higher surface brightness galaxies are older and more metal-rich, suggesting an early and more rapid star formation history for these galaxies. The increasing trends with rotational velocity and total magnitude level off for $V_{\rm rot} \gtrsim 120~{\rm km\,s^{-1}}$ and $M_K \lesssim -23~{\rm mag}$ respectively. This effect is stronger for metallicity (than age) which could reflect a threshold potential above which all metals are retained and thus metallicity saturates at the yield. Outer disk gradients are found to be weaker than the inner gradients as expected for a slower variation of the potential and surface brightness in the outer parts. We find that stronger age gradients are associated with weaker metallicity gradients. Trends in gradients with galaxy parameters are compared with model predictions: these trends do not agree with predictions of semi-analytic models of hierarchical galaxy formation, possibly due to the effect of bar-induced radial flows. The observed trends are in agreement with chemo-spectrophotometric models of spiral galaxy evolution based on CDM-motivated scaling laws but none of the hierarchical merging characteristics, implying a strong dependence of the star formation history of spiral galaxies on the galaxy potential and halo spin parameter.

 $Subject\ headings:\ {\it galaxies: photometry-galaxies: photometry-galaxies: structure}$

1. INTRODUCTION

Color gradients in galaxies reveal information about the nature of their stellar populations via age and metallicity trends, and the amount and distribution of dust. The technique of using broad-band colors as a probe of the stellar populations and star formation histories (SFH) of galaxies, pioneered by, e.g. Searle, Sargent, & Bagnuolo (1973) and Tinsley & Gunn (1976), is still reflected in the modern studies of Peletier & Balcells (1994), de Jong (1996), and Bell & de Jong (2000; hereafter BdJ00). Early analyses, however, suffered sig-

Electronic address: lauren@physics.ubc.ca Electronic address: courteau@astro.queensu.ca Electronic address: bell@mpia-hd.mpg.de Electronic address: holtz@astro.nmsu.edu nificantly from degeneracies between age and metallicity. Worthey (1994) quantified the age-metallicity degeneracy that exists in optical broad-band colors as $\Delta {\rm age}/\Delta Z \sim 3/2$. This implies that the composite spectrum of an old stellar population is nearly indistinguishable from that of a younger but more metal-rich population (and vice versa). This degeneracy can be partially broken with infrared photometry (e.g. H or K band) in addition to optical colors (de Jong 1996). Cardiel et al. (2003) have quantified the relative ability of different color and absorption-line index combinations to constrain physical parameters of composite stellar populations. Their results find that inclusion of an infrared band improves the predictive power of the stellar population diagnostics by $\sim 30 {\rm x}$ over using optical colors alone.

The interpretation of broad-band color gradients also relies on a careful mapping of the dust extinction within a galaxy (Witt, Thronson, & Capuano 1992; de Jong 1996). While dust opacity is much reduced at redder wavelengths, its effects may still be non-negligible in the determination of the stellar content of late-type spiral galaxies and must be considered in the final interpretation of color gradients.

A successful galaxy formation theory must determine the formation timescales for bulges and disks and reproduce the observed stellar ages and chemical distributions in galaxies as a function of galaxy properties. Competing bulge/disk formation scenarios entail distinct structural and kinematic signatures, star formation rates (SFRs), and mixing of the bulge and disk material, that a study of age and metallicity indicators could help disentangle. Current theories for the formation of disk bulges generally fall under two basic pictures: monolithic collapse (e.g. Larson 1974; Calberg 1984) and hierarchical merging (e.g. Kauffmann 1996; Cole et al. 2000). The monolithic dissipative collapse of a gas cloud at high redshift is consistent with strong bulge metallicity gradients (on the order of 0.5 dex/decade within the central ~ 2 kpc, but flattening in the outer parts (Larson 1974)), with metallicity decreasing with increasing radius, shallow positive age gradients (the centers are slightly younger than the outer parts), and old stellar populations. In this "monolithic" scenario the disk would accrete onto the already formed bulge, and thus be younger than the bulge. The dominant signatures in the hierarchical scenario depend on the time evolution of the merger rate: if mergers were most frequent at high redshift, as predicted by presentepoch cosmological models, signatures should be similar to those of dissipative collapse. More recent mergers and tidal disruptions would result in flatter metallicity gradients, and a significant fraction of young or intermediateage stars. In either of the above two scenarios, secular evolution can also drive disk gas and stars to the center via bar instabilities. In general, this scenario predicts that bulges will be similar in metallicity and age and structurally linked to disks (Courteau, de Jong, & Broeils 1996; Courteau 1996). Note, however, that the number of bar formation - gas inflow - star formation - bar dissolution cycles that can occur in a galaxy may be limited, as the central mass formed in the first cycle can prevent subsequent formation of a bar Wyse (1999). ¹ Radial migration of disk material (stars and gas) can also be induced by non-axisymmetric spiral waves (Sellwood & Binney 2002), which would necessarily flatten

Current observational results (O/H gradients, SFRs, constant IMF, gas distribution) favor an inside-out formation for the Milky Way, but the details about age and metallicity gradients in our own Galaxy are conflicting (Freeman & Bland-Hawthorn 2002). Integrated studies of stellar populations in external galaxies can restrict the range of possible interpretations, but formation timescales and chemical evolution of external spiral galaxies have barely been explored (e.g. Matteucci 2002).

metallicity gradients in disks.

These issues have become even more important now that cosmologically-motivated numerical simulations are capable of resolving the formation of disks and bulges. Furthermore, semi-analytic galaxy evolution models use recipes to describe bulge and disk evolution, but if different types of galaxies have different bulge formation mechanisms, these models may give misleading results (e.g. Somerville & Primack 1999; van den Bosch 2000), unless a variety of bulge formation mechanisms are modeled (e.g. Cole et al. 2000).

Existing studies of spiral bulges and disks have placed tentative constraints on the source of their color gradients and which galaxy parameters most strongly correlate with SFHs and, hence, on specific formation scenarios, but some of the results are conflicting. In an study of color gradients in early-type bulges ($\leq \tilde{S}b$) using HST and ground-based data, Peletier et al. (1999) infered that early-type bulges are old (absolute ages not well determined) with a small age spread ($\lesssim 2 \text{ Gyr}$) for all earlytype bulges measured at the bulge effective radius. The old and narrow age range makes it unlikely that these bulges would have formed via secular evolution. The same conclusion does not hold for their (few) later-type galaxies. Peletier et al. (1999) conclude that the intrinsic color gradients of early-type bulges are caused mainly by metallicity gradients (in agreement with other similar studies; e.g. Mehlert et al. 2003), consistent with the monolithic collapse scenario. However, based on the lack of $r^{1/4}$ shaped bulges found in a later study of bulge SB profiles of S0–Sbc galaxies using HST near-IR high resolution imaging, Balcells et al. (2003) have revised their interpretation and conclude that these bulges could not have formed from violent relaxation in mergers, but rather are more consistent with secular formation processes. On the other hand, in an HST study of spatially resolved colors of high redshift ($\bar{z} \sim 0.5$) galaxies in the Hubble Deep Field, Abraham et al. (1999) rule out metallicity gradients as major contributors to galaxy color distributions. They do find, in agreement with Peletier et al. (1999), that large bulges are significantly older than their disks and therefore rule out secular evolution formation processes in favor of a gradual disk formation by accretion of gas. However, the flat metallicity distribution of the bulge is not easily explained in this scenario (particularly since the lack of " $r^{1/4}$ " bulges rules out major merging as a cause of gradient flattening).

The most comprehensive study to date of color gradients in disk galaxies is that of BdJ00, who compute age and metallicity gradients for a sample of 121 nearby lowinclination S0-Sd galaxies. They conclude that galaxy color gradients are due in most part to gradients in age and metallicity in their stellar populations (in the sense that inner regions are older and more metal rich than outer regions) and contend that dust reddening mainly affects the metallicity gradients, but is likely too small to affect their conclusions. In comparing the SFHs with galaxy parameters, they conclude that the SFH of a galaxy is primarily driven by surface density and that the total stellar mass of a galaxy is a less important parameter that correlates significantly with metallicity, but not age. Kauffmann et al. (2003a) also conclude that the recent SFHs, as probed by the $H_{\delta A}$ absorption line index and the 4000Å break, of over 100,000 galaxies are

¹ Only progressively larger bars in the centers of exponential bulges would be allowed to form in a recurring scenario as a result of the disrupting dynamical effect of a growing nucleus (H.-W. Rix 1999, private communication, as reported in Carollo 1999).

more strongly correlated with surface mass density than stellar mass. BdJ00 argued that these correlations could be the result of a surface density-dependent star formation law, coupled with galaxy mass-dependent chemically enriched gas outflows. Bell & Bower (2000) further explored this idea by constructing a family of simple models for spiral galaxy evolution for comparison with the observational trends in SFH with galaxy parameters. Indeed they found that the data are consistent with the proposition that the SFH of a region within a galaxy depends primarily on the local surface density of the gas but that additional ingredients, such as galaxy mass dependent infall(outflow) of primordial(metal-enriched) gas and/or formation epoch, are required to fully explain the observational results.

In spite of genuine progress in recent years in the study of spectro-photometric gradients in spiral galaxies, our ability to model and interpret them in terms of formation models is still limited due to the lack of data and the intricacies involved in converting observed quantities to reliable ages and metallicities. In this study, we use the largest catalog of deep optical and NIR galaxy colors to date to revisit the comparison of broad-band color gradients with stellar population models using a range of SFHs and basic assumptions about the dust distribution. We follow the approach developed by BdJ00, exploring additional parameter ranges and using an extended data base by combining the BdJ00 data with our own collection of deep, optical and NIR surface brightness profiles (Courteau, Holtzman, & MacArthur 2004, in prep.; hereafter Paper III), for a total sample of 172 galaxies. For the combined data base we determine local average ages and metallicities in radial bins for each galaxy and compute gradients in age and metallicity as a function of radius. We pay special attention to the effects of fitting out to different physical extents for individual galaxies and the distinction between inner and outer galaxy gradients. In particular, we find that false trends can be inferred if the radial extent of the gradient fits is not taken into account, which in turn leads to erroneous conclusions about the galaxy parameters that drive their SFHs.

The outline of the paper is as follows. In §2, we describe the data base from which color gradients are computed. Our color gradients are presented in Paper III. and further details of the BdJ00 sample can be found in their §2. In §3 we explore the range of galaxy parameters in our sample and their intrinsic correlations which must be considered when comparing trends in age and metallicity gradients with galaxy parameters. In §4, we discuss the stellar population models to be compared to the data and the different star formation prescriptions adopted. Dust models and its potential effects on our results are discussed in §5. Optical-NIR color-color profiles and their matching population models are presented in §6 and trends with galaxy parameters are explored. The technique by which the data are fitted to the SSP models is presented in §7. Local and global age and metallicities are presented in §8.1 and their gradients are discussed in §8.3 and §8.4 and contrasted with previous results from BdJ00. We conclude with a discussion of the mechanisms that control stellar evolution in spiral galaxies and compare our results with existing models of galaxy evolution in §9.

2. THE DATA

Our data base from which color gradients are measured is a combination of the data in BdJ00 and the compilation by Courteau et al. (2004, in prep., Paper III) of 1063 digital images in the B, V, R, and H passbands of 324 nearby late-type spiral galaxies collected at the Lowell Observatory and Kitt Peak National Observatory. For the current analysis we consider only the face-on and moderately tilted galaxies ($i < 60^{\circ}$) in the sample. All galaxies were selected from the Uppsala General Catalogue of Galaxies (UGC, Nilson 1973) to have: Zwicky magnitude $m_B \leq 15.5$, blue Galactic extinction $A_B = 4 \times E(B-V) \leq 0.5$ (11), and blue major axis $\leq 2'.2$. For the computation of homogeneous structural parameters and color gradients we use the isophotal map determined at R-band and applied onto all other images (BVH) of a galaxy. The SB profiles are reliable (with SB errors $< 0.12 \text{ mag arcsec}^{-2}$) down to $\sim 26 \text{ mag arcsec}^{-2}$ for optical bands and ~ 22 mag arcsec⁻² at H-band. For the purpose of this color-based analysis, we further require that the galaxies have measured surface brightnesses in at least two optical and one near-IR (H) band observations out to at least 1.5 H-band disk scale lengths and with SB errors of less than $0.12 \text{ mag arcsec}^{-2}$. This leaves us with 51 galaxies (25 type I, 17 type II, 9 transition)² with extended reliable color gradients.

Radial profiles were corrected for Galactic extinction using the reddening values of Schlegel et al. (1998). We do not attempt to correct our SB profiles for internal extinction, but discuss the possible effects of dust on our results in §5. The SB profiles were degraded to the worst seeing FWHM before computing color gradients. For a full description of the data see Paper III.

In order to increase the signal-to-noise (S/N) of our color profiles, the SB profiles were averaged into radial bins scaled by the NIR-band disk scale length, $h_{\rm NIR}$, and we required at least 3 data points per bin. The bin sizes were defined as follows:

$$grid_{1}: \qquad grid_{2}:$$

$$0.0 \leq r/h < 0.5, \qquad 0.0 \leq r/h < 0.25,$$

$$0.5 \leq r/h < 1.5, \qquad 0.25 \leq r/h < 0.5,$$

$$1.5 \leq r/h < 2.5, \qquad 0.5 \leq r/h < 0.75,$$

$$2.5 \leq r/h < 3.5, \qquad 0.75 \leq r/h < 1.0,$$

$$3.5 \leq r/h < 4.5, \qquad 1.0 \leq r/h < 1.5,$$

$$4.5 \leq r/h < 5.5 \qquad 1.5 \leq r/h < 2.0,$$

$$2.0 \leq r/h < 3.0$$

The second, finer, grid $(grid_2)$ was used to see if the coarser binning of $grid_1$ hides any important features in the color profiles. The difference in using the two different binnings is small. In particular, this test confirmed that the measured gradients do not depend on the central pixels, which are likely to be more affected by a central concentration of dust in spiral galaxies. Hence we subsequently use $grid_1$ only (as this is the binning of the BdJ00 sample).

² For type I SB profiles (Freeman 1970), the inner profile always lies above the SB of the inward extrapolation of the outer disk, whereas type II systems have a portion of their brightness profiles lying below the inward disk extrapolation. We define a transition case for luminosity profiles that change from type II at optical wavelengths to type I in the infrared. See Paper I for a definition of the different profile types.

Table 1.

Hubble Type	Sa	Sab	Sb	Sbc	Sc	Scd	Sd
mean $H - K$	0.30	0.26	0.30	0.28	0.28	0.24	0.21

NOTE. — Mean 2MASS H - K isophotal colors for non-barred galaxies. Adapted from Figure 16 of Jarrett et al. (2003).

In order to look for trends in color gradients with galaxy parameters, we collected, for as many galaxies as possible, their morphological type, absolute magnitude, H-band disk central surface brightness (CSB), H-band disk scale length, inclination, total H-band magnitude, and rotational velocity $V_{\rm rot}$ (see below). The structural parameters (disk scale length, h, and CSB, μ_0) were computed using our bulge-to-disk decomposition scheme (see Paper I). Total galaxy magnitudes encompass the light out to SB levels given above, and include an extrapolation of the SB profile to infinity with an exponential fit to the last quarter of the SB profile³. The extrapolated magnitude increment (0.07 H-mag on average) is added to the isophotal magnitude which is corrected for Galactic extinction (Schlegel et al. 1998). Stellar masses are computed using the prescription of Bell & de Jong (2001).

We merged our sample with the 121 galaxies from BdJ00 which spans a wider range in Hubble type (S0–Irr) and includes a few low surface brightness (LSB) galaxies. For the computation of color gradients, BdJ00 required at least two optical (BVRI) and one K-band observations per galaxy. The data reductions and radial binning (using only $grid_1$) are very similar to our own. For 3 galaxies in common with both data sets, there is excellent agreement in the overall calibration and radial profiles at least for the BVRH bands (Paper III).

In order to compare the two data sets directly when looking for trends in age and metallicity with galaxy parameters, we converted our H-band magnitudes and surface brightnesses into K-band using the 2MASS H-Kcolor transformations derived from Jarrett et al. (2003). Since we are interested mainly in qualitative trends in age and metallicity with galaxy parameters, coarse transformations are adequate and we took the mean H-K values for each Hubble type, derived from their Figure 16 and listed here in Table 1. The modified H magnitude will be denoted as $H_{\rm m},$ to represent the K-band equivalent of the H-band measurement. We do, however, consider the disk scale lengths in the H and K to be directly comparable. Möllenhoff & Heidt (2001) find $h_J/h_K = 1.01 \pm 0.19$ for a sample of 40 spiral galaxies and the relationship will be even tighter for h_H/h_K , hence a direct comparison of the H and K band disk scale lengths is justified.

It has been suggested that age and metallicity gradients may depend upon the potential of the galaxy and thus vary as a function of $V_{\rm rot}$ (Dalcanton & Bernstein 2002; Garnett 2002a). In order to search for such a trend we augmented out catalog with H I or H α line widths

(which we take to be W50/2, half the line width at 50% peak flux) collected from the literature. These data will enable us to test for a distinct signature in the color profiles from the more prominent dust lanes seen in galaxies with $V_{\rm rot} > 120~{\rm km\,s^{-1}}$ (Dalcanton & Bernstein 2002) and/or if there is a flattening of the metallicity of galaxies above $V_{\rm rot} \sim 150~{\rm km\,s^{-1}}$ (Garnett 2002a). The line widths were collected from various sources and transformations were derived to ensure uniformity between them (see Appendix A). Differences between measurements for a given galaxy for different sources were typically less than 10%, which is sufficient for our purposes.

In order to ensure sufficiently accurate $V_{\rm rot}$ measurements, we restricted our sample to galaxies with inclination greater than 35°. We are left with 98 galaxies in our sample that have reliable rotational velocity measurements.

3. GALAXY PARAMETERS

Trends in age and metallicity (local values and gradients) with galaxy parameters, may bear an imprint from intrinsic correlations within the sample itself. In Figure A1 we plot the galaxy parameters used in this analysis $(h, \mu_0, M_{H_m,K}, \text{ and } V_{\text{rot}})$ against each other. The most notable correlations are the luminosity-rotation speed relation, $M_{H_{\rm m},K}$ versus $\log(V_{\rm rot})$ (the so-called "Tully-Fisher" relation), and the size-luminosity relation, $M_{H_{\rm m},K}$ versus $\log(h)$. All correlations with μ_0 are weaker and have large scatter. In Figure A2 we plot the 4 basic galaxy parameters as a function of morphological type. Trends are seen with galaxy parameters for $T \gtrsim 4$ such that later-type galaxies have smaller rotational velocities and total magnitudes, and lower central surface brightness. On the other hand, there is no clear trend of disk scale length with Hubble type (and hence the trend with total magnitude is largely driven by the trend with CSB, Courteau et al. 2003). Data points are few for T < 4, but deviations from the $T \gtrsim 4$ trends seem to occur. A larger spread is (barely) noticeable in $V_{\rm rot}$, but is further supported by the larger spread in $M_{H_{\rm m},K}$ for which we have more galaxies (unfortunately, reliable $V_{\rm rot}$ s could not be found for the earliest-type galaxies.) The increasing trend in μ_0 with decreasing T seems to level off at T < 4, but the spread is still significant. Finally, earliest-type galaxies have the shortest scale lengths, as expected. We shall return to these correlations in the analysis of trends in age and metallicity gradients ($\S 8$).

4. STELLAR POPULATION MODELS

In order to translate color information into constraints on the underlying ages and abundances of the stellar populations, the color gradients must be compared with stellar population synthesis models. In their most basic form, commonly referred to as simple stellar populations (SSPs), these models provide evolutionary information for a coeval population of stars born with a given composition and initial mass function (IMF). The closest physical analog to such SSPs are globular cluster systems from which the SSP models are calibrated (e.g. Schiavon et al. 2002). Several such SSP models have been produced by a number of independent groups and are in a constant state of modification as improvements to many of the input parameters (e.g. stellar libraries, model atmospheres,

³ This accounts for outer disk truncations that would not be fit properly using the entire profile from our B/D decompositions in Paper I.

convection, mass loss, mixing) come to light. There are discrepancies among the different models that, depending on the application, may result in significantly different interpretations of observations of unresolved stellar populations. In order to determine if these model discrepancies could affect our analysis, we have compared two independent sets of SSPs; the 2003 implementation of the Bruzual & Charlot (2003) models (hereafter referred to as GALAXEV), and the Project d'Étude des Galaxies par Synthèse Évolutive (PEGASE 2.0) models of Fioc & Rocca-Volmerange (1997).

The stellar populations of interest here are those of spiral galaxies spanning the full Hubble sequence (S0-Irr). The approximation of a single evolved stellar population clearly does not apply to evolved, complex stellar populations of spiral galaxies. However, if one assumes that galaxies are composed of a superposition of SSPs, born at different epochs, rates, and metallicities, one can use the SSPs to develop model grids that mimic the range of plausible galactic stellar populations and these can be compared with galaxy color profiles. The stellar population model grids are created by taking the single burst SSPs, with constant stellar IMF and fixed metallicity, and convolving them with a given SFH. A few simplifying assumptions are inherent in this formulation. We are assuming that the IMF does not change as a function of time or galactic environment. The validity of this assumption may be questioned from a theoretical perspective as the IMF is expected to vary systematically with star formation environments (Chabrier 2003, and references therein). However, significant observational evidence of star formation in small molecular clouds, rich and dense massive star-clusters, as well as ancient metalpoor stellar populations, reveals a remarkable uniformity of the IMF (Kroupa 2002). The use of fixed-metallicity SSP implies no chemical evolution. This is clearly an unrealistic assumption with regards to galaxy evolution (as it also ignores feedback effects from stellar winds and supernovae), but it still allows us a reasonable comparison of relative metallicities and ages within and among galaxies (Abraham et al. 1999; BdJ00; Gavazzi et al. 2002).

The specific choice of IMF, parameterized as $\xi(\log m) \propto m^{-x}$, can also potentially affect our results. To gauge the importance of this effect on our color-based analysis we compared model grids obtained with some of the most widely used IMF characterizations; (a) the single-slope Salpeter (1955) with

$$x = 1.35, \qquad 0.1 \le m/M_{\odot} \le 100,$$
 (2)

(b) the Kroupa (2001) IMF (PEGASE models only) with:

$$x_0 = 0.3,$$
 $0.1 \le m/M_{\odot} \le 0.5$
 $x_1 = 1.3,$ $0.5 \le m/M_{\odot} \le 120,$ (3)

and (c) the Chabrier (2003) single-star Galactic disk IMF (GALAXEV models only) which is parameterized as:

$$\xi(\log m) \propto \begin{cases} \exp\left[-\frac{(\log m - \log m_c)^2}{2\sigma^2}\right], & 0.1 \le m/M_{\odot} \le 1; \\ m^{-1.3}, & 1 < m/M_{\odot} \le 100 \end{cases}$$
(4)

The Chabrier (2003) IMF is preferred over the Kroupa (2001) and Salpeter (1955) IMFs because of its better agreement with number counts of brown dwarfs in the galactic disk and its theoretical motivation.

The integrated spectrum, $F_{\lambda}(t)$, of a stellar population with SFR $\Psi(t)$ is computed as the convolution of a single burst stellar population of given metallicity, $f_{\lambda}(t)$, with the given SFR:

$$F_{\lambda}(t) = \int_0^t \Psi(t - t') f_{\lambda}(t') \, \mathrm{d}t'. \tag{5}$$

The left panel in Figure A3 compares the model tracks from the GALAXEV models with the Salpeter (1955) (eq. 2) and Chabrier (2003) (eq. 4) IMFs, and the right panel compares those from the PEGASE models for Salpeter (1955) and Kroupa (2001) (eq. 3) IMFs. The difference between the various IMFs on the model grids are small, thus the specific choice of IMF (within current observational constraints) will not affect our results. We opt to use the Salpeter (1955) IMF for the remainder of this analysis (primarily to facilitate comparison with other studies).

Also over-plotted in the right panel of Figure A3 are the GALAXEV model with Salpeter IMF tracks for direct comparison with the PEGASE model tracks for the same IMF (although note that the upper mass cut-off is $100 \,\mathrm{M}_{\odot}$ in the GALAXEV models and $125 \,\mathrm{M}_{\odot}$ in the PE-GASE models). While differences in the grids between the different models are noticeable (most likely due to different treatments of the thermally pulsing asymptotic giant branch phase, see e.g. Maraston 2003), they are only significant in the bluest regions where the SB errors of our observations are also large (i.e. the outer regions of our spiral galaxies where sky subtraction errors become large, are, for the most part, bluer). Slight differences in the age and metallicity gradients would be inferred using the different models, but we are mainly interested in relative quantities, and thus are not concerned with the small absolute differences between models. For the rest of this analysis we refer only to the GALAXEV models.

We have explored two different SFR regimes, both parameterized by a star formation timescale τ . The first is the simple exponential SFR, $\Psi_{\rm exp}(t)$,

$$\Psi_{\rm exp}(t) = \frac{c_{\rm exp}}{\tau} e^{-t/\tau},\tag{6}$$

where

$$c_{\rm exp} = \frac{1}{1 - e^{-A/\tau}}. (7)$$

The second is the so-called "Sandage" SFR, $\Psi_{San}(t)$ first parameterized by Sandage (1985),

$$\Psi_{\rm San}(t) = c_{\rm San} \frac{t}{\tau^2} e^{-t^2/2\tau^2}$$
 (8)

and

$$c_{\text{San}} = \frac{1}{1 - e^{-1/2(A/\tau)^2}} \tag{9}$$

where $c_{\rm exp}$ and $c_{\rm San}$ are normalization constants (to 1 ${\rm M}_{\odot}$). Figure A4 shows the time evolution of the exponential (top panel) and Sandage SFRs (bottom panel).

The exponential SFR falls off at a given rate for all positive values of τ . However, in order to cover the full color-color space spanned by the observations, negative values of τ were also included which allow for increasing SFRs. The Sandage SFR is characterized by a delayed rise in the SFR, followed by an exponential decline, the rate of which is determined by the value of τ . For values of $\tau > A$, where A is the age of the galaxy (fixed to 13 Gyr in this work), the SFR is still rising at the present time. The average age of a stellar population of a given τ is computed as:

$$\langle A \rangle = A - \frac{\int_0^A t \Psi(t) \, \mathrm{d}t}{\int_0^A \Psi(t) \, \mathrm{d}t}.$$
 (10)

For the exponential SFR, this equates to,

$$\langle A \rangle_{\text{exp}} = A - \tau \frac{1 - e^{-A/\tau} (1 + A/\tau)}{1 - e^{-A/\tau}}$$
 (11)

and for the Sandage SFR,

$$\langle A \rangle_{\text{San}} = A - \frac{-Ae^{-\frac{1}{2}\frac{A^2}{\tau^2}} + \frac{1}{2}\tau\sqrt{2\pi}\operatorname{erf}\left(\frac{A}{\sqrt{2\tau}}\right)}{1 - e^{-\frac{1}{2}\frac{A^2}{\tau^2}}}.$$
 (12)

Figure A5 shows the resulting model grids for the exponential (blue), and Sandage (red) SFRs overlaid on each other. Lines of constant average age $\langle A \rangle$ are the dashed, roughly vertical lines (labeled in Gyr), while lines of constant metallicity are solid and run closer to the horizontal (labeled in Z, the mass fraction in elements heavier than helium, where $Z_{\odot}=0.02$). The overall shape of the two model grids are quite similar, the main difference being that the Sandage SFH has a younger average age for a given B-R and the metallicity is slightly higher for a given R-H. The Sandage grids also cover a wider range in ages (which would increase the magnitude of our measured age gradients).

The reported radial age gradients inferred from color gradients (e.g. BdJ00) seem to be at odds with the lack of age gradient observed in open clusters of the Galaxy (Freeman & Bland-Hawthorn 2002). Would it be possible that the apparent radial age gradients observed in spiral galaxies are simply due to small amounts of young frostings of star formation on top of an underlying old population? In order to test for such effects in our age determinations, we produced new model grids for the same underlying SFH but with an additional burst of star formation at different times and fractional masses. The burst was added as a Sandage (1985) type profile (eq. 8) with $\tau = 0.1^4$. The average age for the models with a burst superimposed on the underlying SFR is now computed as,

$$\langle A \rangle = A - \frac{(1 - b_f) \int_0^A t \Psi(t) \, dt + b_f \int_{t_b}^A t' \Psi_b(t') \, dt}{(1 - b_f) \int_0^A \Psi(t) \, dt + b_f \int_{t_b}^A \Psi_b(t') \, dt}$$
(13)

where b_f is the mass fraction of the burst, t_b is the time since the burst, i.e. the burst of star formation occurs t_b Gyr before the current age of the galaxy, A, and

 $t' = t - t_b$. Figures A6 and A7 demonstrate the effect of such a burst of star formation superimposed on an underlying exponential SFR with ages (t_b) of 1 and 4 Gyr respectively. The left panel in both figures shows the effect if 10% of the galaxy's total mass was involved in the burst, and the right panel shows a 50% (by mass) burst. The models certainly do not cover the same extent in the color-color space for recent bursts. With only 10% of the total galaxy mass in the burst (Fig. A6; left panel) the grid does not extend to the red as far as those without bursts. The effect is strongest ($\sim 0.3 \text{ mag}$) in the optical colors. Also, the burst grid does not extend as far into the blue optical colors ($\lesssim 0.1 \text{ mag}$) for the most metal-rich galaxies. This is because we are essentially adding more older stars to the SFHs that are rising at 13 Gyr ($\tau < 0$ for Ψ_{exp} , or $\tau > 13$ Gyr for Ψ_{San} ; This effect is stronger at higher metallicity because the evolution of B-R color with time steepens for higher metallicity stellar populations at ages $\sim 1-3$ Gyr in the GALAXEV models.) The lines of constant age also steepen. "Frosting" also shifts the R-H colors to redder values ($\sim 0.1 \text{ mag}$) at a given metallicity. This, in fact, prevents the burst grid from reaching red-ward enough as required by the observational data for the inner-most parts of the galaxies (see Figs. A9–A13). Either the bursts are accompanied by significant amounts of dust, or 1 Gyr old bursts can be ruled out for the central parts of late-type galaxies. The 50% by mass burst in Figure A6, right panel, shows that the grid covers only a narrow range in color-color space that does not extend far enough into the red or the blue to agree with the observations. For older bursts of star formation, the model grids have colors fully consistent with the no-burst models. This is shown in Figure A7 for a pure exponential SFH (blue) overlaid with an exponential plus $t_{burst} = 4$ Gyr Sandage-like burst (red). The grids are almost identical with respect to their shape and location (with slight narrowing of the 50% mass burst grid). The only difference is the average ages (eqs. 10 & 13), being younger for a given color of the burst grid. Thus, adding a burst of star formation that is older than ~ 1 Gyr has a similar effect as changing the overall form of the SFH; the grid shape and color coverage are the same, but the average age can change significantly from one scenario to another. Not only do the age determinations change, but the age gradients can also be different for a given SFH (compare Sandage and exponential SFH) model grids in Fig. A5). Since the actual SFHs of real galaxies are unknown, the absolute values of the gradients measured with this color-based technique cannot be trusted. We can, however, trust that a gradient exists in a galaxy, but not its magnitude. We can also compare relative gradients among different galaxies if we assume self-similar SFHs and no significant bursts of star formation within the last 1–2 Gyr.

A reasonable estimate of the validity of this assumption can be obtained from the study of Kauffmann et al. (2003a) who used the $H\delta_A$ absorption line index and the 4000Å break age indicators along with the Bruzual & Charlot SSPs to constrain the SFHs, dust attenuation, and stellar masses of over 100,000 galaxies from the Sloan Digital Sky Survey (SDSS). For each galaxy they estimated F_{burst} , the fraction of the total stellar mass formed in bursts in the past 1-2 Gyr. Their Figure 5

⁴ This timescale is justified on the basis that starbursts are consistent with a constant SF lasting 10–100 Myr (Meurer 2000).

shows the fraction of galaxies with ${\rm F}_{burst}>0$ at the 50% and 97.5% confidence levels in stellar mass bins ranging from 8.0– $12.0\log_{10}(M_{\odot})$. From this and estimates of the galaxy stellar masses (Bell & de Jong 2001), we infer the fraction of galaxies in our sample that have undergone bursts of SF in the past 1–2 Gyr is $\sim 1\%$ ($\sim 12\%$) at the 97.5% (50%) confidence level. The fraction of galaxies that have ${\rm F}_{burst}\gg 10\%$ will be even smaller and we conclude that our assumption of no recent burst is valid.

5. DUST EFFECTS

While the presence of dust in late-type spiral galaxies is well-established, its distribution and effective optical depth remain poorly constrained. Extinction by dust could potentially mimic a color gradient and its effects must be considered in determining the stellar content of galaxies from colors. We attempt to quantify the effects of dust extinction on colors with simple dust geometry extinction models, adopting the MW extinction curve and albedo values from Gordon, Calzetti, & Witt (1997). The extinction vector for the simplistic foreground screen model with $A_V = 0.3$ is shown (as the arrow) in the upper left corner in Figures A9–A13. The vector is in the same general direction as the observed gradients of the galaxies, but given the unrealistic nature of this model, we do not consider it further (but include it for visual comparison). Also shown in the top left corner in Figures A9-A13 is the more realistic "face-on triplex" dust model of Disney, Davies, & Phillipps (1989) and Evans (1994). This model assumes that the stars and dust have exponential distributions in both the radial and vertical directions with radial scale lengths h_* and h_d , and vertical scale lengths z_* and z_d . Although scattering is not taken into account, Byun, Freeman, & Kylafis (1994) and de Jong (1996) have shown that its effects are negligible in face-on galaxies (as photons are just as likely to be scattered into the line of sight as they are out of it.) We therefore use the dust absorption curve to compute the dust optical depth;

$$\tau_{\lambda}(0) = \frac{\tau_{\lambda}}{\tau_{V}} \tau_{V}(0) (1 - a_{\lambda}) \tag{14}$$

where τ_{λ} and a_{λ} are the dust optical depth and albedo respectively.

Studies of multi-wavelength data that solve simultaneously for the intrinsic color of stellar populations and reddening and extinction effects from dust find central optical depths, $\tau_V(0)$, in the range 0.3–2.5 for types Sab-Sc (Peletier et al. 1995; Kuchinski et al. 1998; Xilouris et al. 1999). The HST and ground-based color gradient study of early-type bulges (\leq Sb) by Peletier et al. (1999) reveals dust extinctions of $A_V = 0.6-1.0$ mag (or $A_H =$ 0.1–0.2 mag) in galaxy centers but negligible extinction beyond one effective radius. Multi-band SB profile modeling of massive edge-on disks suggests that the dust is confined to a thin extended plane, with $z_d/z_* \lesssim 0.7$ and $h_d/h_* \sim 1.4$ (Xilouris et al. 1999; Matthews & Wood 2001). Masters, Giovanelli, & Haynes (2003) studied internal extinction in the near-IR for a sample of 15,244 2MASS galaxies by looking at the inclination dependence of various photometric parameters, and concluded that galaxies with $M_{\lambda} - 5\log(h) > -20$, -20.7, and -20.9 in the J, H, and K_s -bands respectively are spared any extinction, but that disk opacity increases monotonically

with disk luminosity. Application of the triplex model for these galaxies favors small dust-to-star scale height ratios ($z_d/z_* \sim 0.5$, in good agreement with Xilouris et al. 1999) and face-on central opacities of $\tau^{\circ}(0) = 0.7, 0.3$ at H and K_s respectively.

We adopt the same vertical and radial scale length ratios for the dust and stars; using $z_d/z_* = 0.7$ and $h_d/h_* = 1.4$ instead stretches the gradients by only 0.018 in B - R, 0.019 in R - H, and 0.021 in R - K, and the central V-band optical depth to $\tau_V(0) = 1$ (or pole-to-pole V-band optical depth of 2). The higher end of the measured range of $\tau_V(0) = 2$ is shown in the upper left corner of Figures A10 & A11 (right panels).

The triplex models lie parallel to, and thus could contribute significantly to, the observed gradients (note there is no overall calibration in the dust models so they can slide to any region on the plot). For the gradients to be entirely due to dust requires extremely high central optical depths $(\tau_V(0) \sim 5)$ to reproduce the data. Also, the triplex models alone cannot reproduce the significant color gradients observed from the half-light radius (denoted by open circles) outward. Thus, while dust is likely a contributor to color gradients, age and metallicity effects must also be invoked.

Dalcanton & Bernstein (2002) have analysed optical and infrared color maps of 47 extremely late-type (bulgeless) edge-on spirals spanning a wide mass range (40 < V_c < 250 km s⁻¹). They find that higher mass (rotation velocity) galaxies have more prominent dust lanes and have redder colors than the stellar population grids (whereas the less massive galaxies have colors consistent with the population grids). Analysis of their $R-K_s$ color maps, and a comparison of colors between their edge-on sample and the face-on sample of de Jong (1996) suggests that dust plays little role in all but the most massive galaxies in their sample ($V_c > 120 \text{ km s}^{-1}$).

Previous analyses have ruled out dust effects on the color gradients in galaxies based on the fact that they see no correlation between the gradients and inclination. Dust effects on gradient profiles as a function of bulge-to-total ratio (B/T) and inclination were modeled by Byun, Freeman, & Kylafis (1994). Their Figure 6 shows B-I versus radius for model galaxies with different B/T ratios and $\tau_V(0)$ ranging from 0.0–10.0 for inclinations 0–85°. In the 0–50° range the differences in the profiles are very small and would not be detected in the observations. Our measured radial gradients also show no inclination dependence, but we do not consider this grounds to rule out significant dust extinction.

Based on optical-IR imaging of S0–Sbc galaxies, Peletier & Balcells (1996) found that "dust-free" colors of galaxy disks are not significantly different from their bulges. They derived bulge colors from minoraxis wedges in images of early-type edge-on spirals. The wedges are presumed dust-free above the disk plane. They conclude that (dust-free) bulge and disk colors are very similar with $\Delta(B-R)=0.045\pm0.097$ and $\Delta(R-K)=0.078\pm0.165$. We find a significantly different result; as can be seen in Figure A8 (compare with Fig. 2 in Peletier & Balcells 1996), our bulges are much redder than their disks with $\Delta(B-R)=0.29\pm0.17$ as $\Delta(R-K)=0.30\pm0.17$. This could be due to genuine dust extinction in our galaxies or there is a fundamental difference between our respective samples and/or

analysis methods. Their disk SB profiles were measured along 10°-wide wedge apertures centered 15° away from the disk major axis, to avoid the prominent dust lanes near the major axis of their inclined galaxies. Naturally, this technique is sensitive to a vertical disk color gradient. Dalcanton & Bernstein (2002) have suggested that all thin disks are embedded in a red stellar envelope. Whether this envelope is redder or bluer than the thin disk depends on the rotational velocity of the galaxy: redder envelopes for $V_{rot} < 120 \text{ km s}^{-1}$ and bluer otherwise, but the color of the envelope is similar for all disk galaxies. The redder thin disks of the galaxies with $V_{rot} > 120 \text{ km s}^{-1}$ are attributed to strong dust lanes observed in their B-R color maps, which disappear in the $V_{rot}<120~{\rm km\,s^{-1}}$ galaxies. Clearly, these red stellar envelopes, and hence the presence of vertical color gradients in disk galaxies renders the interpretation of Peletier & Balcells (1996) "disk" colors difficult. The 10° offset from the major axis may result in a measurement of the "red envelope" stars which are intrinsically older than the thin disk stars (though not necessarily redder since thin disk stars could be reddened by a central dust lane).

While optical-IR color imaging alone is not sufficient to break the degeneracy between dust and stellar population effects on the color gradients, the tentative consensus to date is that dust is generally not a significant contributor to galaxy colors in low-mass/low-luminosity spiral galaxies, but is likely important in more massive/brighter galaxies. It must be borne iin mind that future studies of high-resolution IR and FIR imaging and absorption-line spectroscopy may radically alter this view.

6. COLOR-COLOR PROFILES

Optical-NIR color-color profiles are shown for the Courteau et al. sample of in Figures A9–A10 and A12– A13 (see Figs. 1–5 in BdJ00 for similar plots with their sample and our Fig. A11 which is only a subset of the BdJ00 sample with available $V_{\rm rot}$ valuess). Typical observation errors are shown as crosses in the lower right corners of Figures A9–A13. From left to right the crosses represent calibration errors, and average sky subtraction errors for the innermost and outermost bins. The galaxy centers are indicated by solid symbols: circles for type-I galaxies, triangles for type-II, and asterisks for transition galaxies (as defined in Paper I). Open circles denote the half-light radius of the disk. The line types for the galaxy color profiles represent bar strength: solid for barless (A), dashed for mild bars (AB), and dot-dashed for strong bars (B). It is conceivable that the type-II "dip" could be due to dust extinction and/or stellar population effects, possibly linked to the presence of a bar, and or inner-disk truncation (see Paper I). However, we do not see any distinction between the different SB profile types in the color gradients. This argues against dust as a major factor for the type-II phenomenon as dustier galaxies would be redder and have larger gradients. No conclusion can be drawn about the effects of a bar due to the small size of our sample and the fact that non-barred galaxies may have once harbored a bar that dissolved after mixing the stellar population.

Over-plotted on Figures A9–A13 are our convolved Bruzual & Charlot (GALAXEV) stellar population models with an exponential SFH at different metallicities.

Lines of constant average age $\langle A \rangle$ (see eq. 10) are the dashed, roughly vertical lines, while lines of constant metallicity are solid and nearly horizontal. In the upper left corner, triplex and foreground screen dust models are plotted with the galaxy center and disk half-light radius denoted by solid and open circles respectively. All of the galaxies show significant color gradients that are consistent with gradients in both age and metallicity with the central parts having older mean ages and being more metal rich. Figures A10 & A11 for the Courteau et al. and BdJ00 samples reveal a largely consistent picture of the radially-resolved colors of spiral galaxies, though the Courteau et al. galaxies extend to higher metallicity (0.1– 0.2 mag in R - H). The origin of this discrepancy is not clear, but we note that the optical versus J-K colors of galaxies are not well fit by single metallicity models (e.g., Fig. 15 of Bell et al. 2003). It may well be that, due to TP-AGB prescriptions, systematic errors of 0.2 mag between H and K predicted colors are inevitable. Thermal emission from the telescope at K-band may also affect sky flats of the type used by BdJ00. Bearing in mind these potential sources of systematic uncertainty, we feel that the degree of similarity between the Courteau et al. and BdJ00 galaxy samples is satisfying.

The small number of earlier-type galaxies (Sab–Sbc) in our sample makes it difficult to infer any trends in age and metallicity with galaxy type, but Figure A28 shows hints that later-types are slightly less metal-rich than the earlier types.

In Figures A10 & A11 we divide the Courteau et al. and BdJ00 samples, respectively, at $V_{\rm rot} \leq 120 \, \rm km \, s^{-1}$, the threshold above which all edge-on galaxies have prominent central dust lanes (Dalcanton & Bernstein 2002). Due to inclination restrictions, we could only retrieve reliable H I line-widths for 28 of our 51 galaxies and 70 out of the 121 BdJ00 sample. A trend with $V_{\rm rot}$ is detected in Figures A10 & A11 with faster rotators being more metal rich and having older mean ages; also consistent with them having a higher dust content. However, according to the triplex models, the true signature of dust is not simply a redder color, but also a stretched color profile (compare triplex profiles in Figures A10 & A11 for V-band optical depths of $\tau_V(0) = 1$, left panels, and $\tau_V(0) = 2$, right panels). For our sample (Fig. A10), the length of the gradients appears to be about the same in both velocity bins. For the BdJ00 sample (Fig. A11) the gradients could be more extended in the larger $V_{\rm rot}$ bin, but the stretching is not predominantly along the R-Kaxis, as in the triplex dust models. Clearly we cannot attribute with absolute certainty the redder colors of the faster rotators to dust effects.

7. MODEL FITTING

Ages and metallicities are determined by fitting the SPS models to the radial galaxy colors using a maximum-likelihood approach similar to that of BdJ00 (see their §3 for further details). We compute a finely spaced grid in τ using equations 5 & 6, and interpolate (linearly) between the SPS metallicities. Treating the colors and errors of each annulus separately, we compute an average age and metallicity per annulus by minimizing the χ^2 statistic:

$$\chi^{2} = \frac{1}{N-1} \sum_{i=1}^{N} \frac{(\mu_{\text{obs},i} - \mu_{\text{model},i}(\langle A \rangle, Z) - \mu_{c})^{2}}{\delta \mu_{\text{tot},i}^{2}}, \quad (15)$$

where N is the number of passbands (at least 3; 2 optical plus 1 IR), $\delta \mu_{\text{tot},i}$ is the total error in passband i, and μ_c is the best normalization between the model and data computed as a weighted average:

$$\mu_c = \frac{\sum_{i=1}^{N} \frac{(\mu_{\text{obs},i} - \mu_{\text{model},i}(\langle A \rangle, Z) - \mu_c)^2}{\delta \mu_{\text{tot},i}^2}}{\sum_{i=1}^{N} \frac{1}{\delta \mu_{\text{tot},i}^2}}.$$
 (16)

Errors for the individual age and metallicity measurements as well as their gradients are estimated using a Monte Carlo approach. One hundred realizations of the model fits are obtained for each radial bin using errors drawn from a normal distribution of the observational errors (which include calibration, sky subtraction, and flat fielding errors added in quadrature). For each realization, gradients are computed as weighted linear fits to the parameter (age and metallicity) determinations as a function of the radial scale length. The weights in the fits are taken as the $\Delta \chi^2 = 1$ interval for each annulus–model fit. The error for the measured gradients and individual ages and metallicities are taken as half the interval containing 68% of the 100 Monte Carlo realizations (i.e. the 1σ confidence interval).

A few galaxies in both samples fall outside the model grids and thus cannot be fit reliably. These were removed from the sample for the model fits, but are worthy of some discussion. As can be seen in Figure A9, five of our galaxies lie significantly red-ward of the model grids in their central R-H color. The dust vector indicates that such red colors could result from a central dust concentration. Another explanation could be an extremely (unrealistically) metal-rich central stellar population. Three of our galaxies lie considerably red-ward of the model grids in their B - R colors. Given the current WMAP measurement of the age of the universe (13.7 Gyr; Spergel et al. 2003), it would be unrealistic for these galaxies to have extremely old central regions. Dust likely contributes to the red colors, but they could also result from erroneous seeing measurements. In the BdJ00 sample 3 very late-type (Sdm/Irr) galaxies (see left panel of Fig. A11) and the extended tails of another 3 galaxies lie blue-ward of the model grids in their R - K colors. These low surface brightness galaxies may suffer from calibration andsky uncertainties couple with the weakness of the model predictions at such low metallicities. Finally, the BdJ00 sample has 3 early-type galaxies whose entire profiles lie red-ward of the grids in their B-Rcolors. Again, extremely old ages are improbable, but significant dust absorption could contribute to the red colors of these three galaxies. Thus, unlike some of the studies cited in §5, these observations remind us of our fragile understanding of dust effects and the challenge we face in trying to separate them from stellar population effects.

8. RESULTS

8.1. Local and Global Trends in Age and Metallicity

Figure A14 shows the local average age (left) and metallicity (right) as a function of local surface brightness. There is a clear trend in the local age and metallicity as a function of local SB in the sense that regions of higher SB are older and more metal rich, but with large scatter, as also found in BdJ00. This correlation suggests that the local potential plays an important role in the SFH.

Figure A15 shows an effective average age, $\langle A \rangle_{\text{eff}}$, for a galaxy, taken as the measured mean age in the 0.5-1.5h averaged radial bin, as a function of central surface brightness (left plot) and total galaxy magnitude (right plot). There is a clear trend in $\langle A \rangle_{\text{eff}}$ as a function of both $\mu_{0,H_{\rm m},K}$ and $M_{H_{\rm m},K}$ with more luminous and higher CSB galaxies having older $\langle A \rangle_{\text{eff}}$ (as expected from Fig. A14). However, in both cases, the roughly linear increasing trend at $\mu_{0,H_{\rm m},K}\gtrsim 18.5$ mag arcsec⁻² and $M_{H_{\rm m},K}\gtrsim -22.5$ mag seem to flatten for brighter values. For $M_{H_{\rm m},K}\lesssim -22.5$ there is large scatter and a much weaker (if any) trend of increasing age with total magnitude (but still containing the oldest galaxies). In Figure A16 we plot $\langle A \rangle_{\text{eff}}$ as a function of $h_{H,K}$ (left) and $V_{\rm rot}$ (right). As expected from the correlation of $M_{H_{\rm m},K}$ with V_{rot} (Fig. A1), a trend of increasing $\langle A \rangle_{\text{eff}}$ with $V_{\rm rot}$ is detected with a similar turnover in the slope of the correlation at higher rotational velocities ($V_{\rm rot} \gtrsim 120$ km s⁻¹, the location of the vertical dotted line). The left panel of Figure A16 may show a weak trend of increasing age with h, however, the scatter is very large. Note also that the spread in age is larger for smaller h galaxies, and reduces with increasing h.

Figures A17 & A18 similar trends for the effective metallicity, $\log(Z_{\rm eff}/Z_{\odot})$ versus $\mu_{0,H_{\rm m},K},~M_{H_{\rm m},K},$ and $V_{\rm rot},$ but no trends are seen with h. Effective metallicity increases with total magnitude up to $M_{H_{\rm m},K}\sim-22,$ but likely saturates for brighter galaxies at roughly solar metallicity (with large scatter). Similarly, in the right panel of Figure A18, $\log(Z_{\rm eff}/Z_{\odot})$ increases with $V_{\rm rot}$ up to $\sim120~{\rm km\,s^{-1}}$ and then levels off with smaller scatter. There is no dependence of $\log(Z_{\rm eff}/Z_{\odot})$ with h.

8.2. Global Trends in Age and Metallicity Gradients

One of the conclusions from BdJ00 is that the amplitude of the age gradients increases from HSB to LSB galaxies. However, this is likely an artifact of their linear gradient fitting technique out to different number of radial bins (scaled by the galaxy disk scale length), anywhere from 2–4 bins (i.e. out to 1.5–3.5 scale lengths). Assuming that the LSB galaxy photometry generally does not extend to as many scale lengths as the HSB photometry, non-linear gradients in the galaxies (e.g. steeper in the inner regions, flattening at large radii), could mimic a trend with SB. To demonstrate this, in Figures A19 & A20, we plot average age, $\langle A \rangle$, and metallicity, $\log(Z/Z_{\odot})$, respectively, as a function of radius. In each case, the left panels give radius in terms of disk scale lengths, and the right panels have the physical radius in kpc. Modulo fairly large uncertainties, we see that gradients are not linear over the extent of the galaxy. The inner and outer slopes are often quite different, sometimes even changing sign. Also, the galaxies are not all measured out to the same number of scale lengths. When plotted against number of scale lengths, most galaxies have steeper (negative) inner gradients that flatten off,

or even turn around, in the outer parts. With the exception of extremely early or late-types, the outer slopes are quite similar for most galaxies. However, when plotted as a function of physical scale (kpc), the slopes can be quite different, with a rough trend for the earliest types being steepest, and leveling off for later-types.

Figures A19 & A20 demonstrate that fitting gradients out to a different number of scale lengths yields misleading results. In general, the larger the fit baseline, the shallower the measured gradient. We verify this assertion in Figure A21 where we plot age gradients fit out to different numbers of radial bins for all the galaxies as a function of CSB (0–1.5 $h_{H,K}$ (top left), 0–2.5 $h_{H,K}$ (top right), 0–3.5 $h_{H,K}$ (bottom left), and 0–4.5 $h_{H,K}$ (bottom right)). Indeed, fitting fewer bins results in systematically larger (usually negative, but occasionally positive) age gradients. The more extended the baseline, the flatter the gradient. LSB galaxy profiles do not extend as far as HSBs (in scale lengths, as indicated by the lower CSB galaxies dropping out of the longer baseline fits) and thus appear to have larger gradients.

Given the dangers of fitting gradients out to different radial extents, in the remainder of this analysis we consider "inner" and "outer" gradients fitted over the $1^{st}-2^{nd}$ radial bins and $2^{nd}-4^{th}$ bins, respectively⁵. This restriction greatly reduces the available galaxy parameter range, especially for the LSB galaxies. Also note that inner gradients will be much more affected by dust (if present) than outer gradients.

8.3. Age gradients

In Figure A22 we plot the inner (left panels) and outer (right panels) gradients measured in disk scale lengths (upper panels) and kpc (lower panels) as a function of CSB (left plot) and total magnitude (right plot). Unlike BdJ00, we do not see a trend of $d\langle A \rangle / dr$ (Gyr/h) (inner or outer) with CSB. Note that the low CSB galaxies are missing in the outer gradient plots so one cannot assess any trend for the outer gradients with great confidence. The current data suggest that outer gradients are generally smaller than those within. When age gradients are plotted as a function of kpc, the inner gradients are slightly steeper for higher CSB galaxies $(\mu_{0,H_{\rm m},K} \lesssim 17.5)$. The 3–4 outliers at high positive gradients are the S0 galaxies whose color gradients are inverted (bluer inward). Such anomalous gradients have been seen before in S0 galaxies (e.g. Emsellem et al. 2002) and are often interpreted as the result of a recent gaseous accretion followed by (central) star formation. These are also the few galaxies that deviate to much younger ages from the general trend of decreasing effective age with galaxy type (see left plot of Fig. A27) which would agree with the above interpretation of recent accretion and SF.

There is a slight trend (with large scatter) for more luminous galaxies to have steeper $d\langle A \rangle/dr$ (Gyr/h) negative gradients (inner and outer), and the fainter galaxies extending to positive gradients. However, this trend disappears when the gradients are plotted as a function of kpc. In this scale the outer gradients are greatest (negative or positive) for the fainter galaxies, and become

negligible for the brighter ones. A similar, somewhat stronger trend of steepening gradient (in scale lengths) with increasing disk scale length is seen in Figure A23 (left). The trend in $\mathrm{d}\langle A \rangle/\mathrm{dr}$ (Gyr/kpc) is reversed (ignoring the 3–4 steep positive gradient points) such that bigger galaxies have smaller gradients. This may reflect the larger galaxies as being less likely to have had any recent activity/interactions, as the small gradients combined with the older ages for the bigger galaxies suggest an overall old age for the largest galaxies. Similar trends are seen with $V_{\rm rot}$ (as expected from the correlations between $V_{\rm rot}$ with h and M in Fig. A1), but they are weaker (largely because of the smaller sample).

8.4. Metallicity gradients

Figures A24 & A25 recast the information presented in Figures A22 & A23 discussed above, but now in terms of metallicity gradients.

Metallicity gradients are less well measured and are more sensitive to dust effects than age gradients (according to the triplex dust models discussed in $\S 5$). Nevertheless, the trends in the metallicity gradients with galaxy parameters are very similar to those with age gradients (see $\S 8.3$). The trends in the magnitudes of the gradients as a function of galaxy parameters are comparable except the correlation changes sign. This suggests a direct anticorrelation between age and metallicity gradients within a galaxy which is seen in Figure A26 (although with some scatter), such that stronger age gradients are associated with weaker metallicity gradients (and vice versa).

9. DISCUSSION

Our main findings can be summarized as follows:

- (i) Our relative age determinations are robust under the assumption that the underlying SFR of all disk galaxies is similar, and that no major star bursts have occurred in the past 1–2 Gyr (which is justified on the basis of Kauffmann et al. (2003)).
- (ii) Dust cannot be ruled out as a contributor to color gradients in spiral galaxies, although it is unlikely that the gradients are largely due to dust extinction.
- (iii) Age and metallicity correlate strongly with local surface brightness: higher SB regions tend to be older and more metal-rich (see Fig. A14). This indicates that the local potential plays a significant role in the SFH of spiral galaxies.
- (iv) Age and metallicity, measured at an effective radius of 1h, increase with earlier Hubble type, $M_{H_{\rm m},K}$, $V_{\rm rot}$, and $\mu_{0,H_{\rm m},K}$ but the trends flatten for $T\lesssim 4$, $M_{H_{\rm m},K}\lesssim -22.5$ mag, $V_{\rm rot}\gtrsim 120$ km s⁻¹, and $\mu_{0,H_{\rm m},K}\lesssim 18.5$ mag arcsec⁻² (see Figs. A15–A18 & A27). Age also correlates weakly with scale length (with scatter decreasing with galaxy size, see right plot of Fig. A16).
- (v) Age and, to a lesser extent, metallicity gradients show radial structure, with generally steeper gradients in the inner parts of the galaxy. Care must thus be taken when defining the gradient fit region (see Figs. A19–A21).

 $^{^5}$ Note that these two definitions cannot be interpreted as bulge and disk gradients as the inner fit goes out to 1.5 disk scale lengths, and bulge scale lengths are typically ${\sim}0.13~h_d$ (Paper I).

- (vi) Age gradients, as measured as a function of scale length, show correlations with luminosity, size, and rotational velocity (Fig. A22), especially in the inner disk. Trends in metallicity gradients with galaxy parameters are weaker (Figs. A24 & A25).
- (vii) Age gradients do not correlate with CSB, contrary to the findings of BdJ00, which we attribute to inconsistencies in their fit radii (see left plot of Fig. A22). This is not at odds with statement (iii) since μ_0 and h are not strongly correlated.

These observations are consistent with a picture where (i) higher surface brightness regions of galaxies formed their stars earlier than lower surface brightness regions, or at a similar epoch but on shorter timescales, and (ii) the SFHs at a given SB level, which lead to age gradients, are modulated by the overall potential of the galaxy such that brighter/higher rotational velocity galaxies formed earlier. These trends reach saturation for the brightest and highest CSB galaxies.

An earlier formation time for more massive galaxies is clearly in conflict with hierarchical galaxy formation which predicts that more massive galaxies form late. This discrepancy could be remedied if there is a mechanism at work that prevents the gas in lower mass galaxies from cooling and forming stars at early times. Feedback processes are often invoked as a possible solution, but no prescription has been found thus far that agrees with all observational constraints (e.g. Kauffmann et al. 2003; Bell et al. 2003).

In a related manner, the semi-analytic models of hierarchical galaxy formation of Kauffman (1996) predict a correlation between bulge-to-disk ratio and luminosityweighted age, such that the bulges of late-type spirals should be older (up to ~ 4 Gyr) than those of earlytype spirals, although this correlation could be erased by any significant inflow from the disk after the last major merger. Figure A27 (left) shows a strong correlation of effective age with galaxy type, but in the opposite sense of Kauffmann's prediction; later-type galaxies have systematically younger effective ages. Clearly, mixing by a bar could erase the predicted age trend. If bars trigger radial flows the gradients of strongly barred galaxies would be flat (the flattening would occur on short enough timescales). To look for such mixing effects, we plot age and metallicity gradients as a function of barredness in Figure A29. No trends are seen when the gradients are plotted in scale lengths, but against kpc, the strongly barred galaxies may have smaller age gradients (inner and outer), though this observation is based on small statistics. This agrees with Martin & Roy (1994) who found similar flattening of O/H metallicity gradients with bar strength (their trend also disappears when the gradients are plotted in scale lengths). Thus, under all assumptions, our observations cannot be reproduced by the Kauffmann (1996) models. The same model deficiency responsible for the backwards age-size correlation, as compared against observations, could also be the cause of the discrepancy in bulge morphology versus age seen in the Kauffmann (1996) models.

Prantzos & Boissier (2000; hereafter PB00) present chemo-spectrophotometric models of spiral galaxy evolution. They adopt a Schmidt-type law for the SFR, which is proportional to the gas surface density and varies with

galactocentric radius (dynamical time), assume an inflow rate (of unenriched gas) that decreases exponentially with time and increases with surface density and galaxy mass, and assume that the gas settles into an exponential disk (bulges are not modeled), but do not consider radial flows (e.g. by viscosity which could create gradients, or due to a bar which could flatten radial gradients on small timescales). The star formation efficiency and infall rate are free parameters tuned to match the Milky Way observational constraints. The models are then extended to other disk galaxies by adopting the Cold Dark Matter(CDM)-based scaling relations of Mo, Mao, & White (1998). As such, their galaxy disk radial profiles are fully described by just two parameters: rotational velocity, $V_{\rm rot}$ (assuming a constant disk-to-halo mass ratio), and the halo spin parameter, λ . A third parameter describing the formation redshift would be required for a description fully consistent with the CDM hierarchical models of galaxy formation but, as of yet, there is no clear definition for the time of formation for an individual galaxy. Hence, PB00 assume that all galaxies started forming at the same epoch (13.5 Gyr ago) but evolve at different rates.

The PB00 models give predictions for O/H abundances and gradients that as could be measured in bright H II regions in nearby galaxies. Note that O/H determinations in H II regions probe the present-day ISM abundances and are insensitive to abundance evolution with time. Still, their model predictions and observations of O/H gradients can be compared, at least indirectly, to our stellar luminosity weighted gradients. PB00 find that the absolute central abundance for a given $\lambda \geq 0.03$ correlates with $V_{\rm rot}$ (and total magnitude) such that faster rotators have larger central abundances, but the trend saturates for $V_{\rm rot} \gtrsim 220~{\rm km\,s^{-1}}$. Furthermore, at a given $V_{\rm rot}$, the central abundance decreases with increasing λ but again saturates for galaxies with $V_{\rm rot} \gtrsim 220~{\rm km\,s^{-1}}$ above which central abundances are high, regardless of λ . By extension, we should see a trend of increasing central abundance with $V_{\rm rot}$, with significant spread (larger at lower $V_{\rm rot}$) due to different values of λ , but this trend would flatten and show less dispersion above $V_{\rm rot} \gtrsim 220$ ${\rm km \, s^{-1}}$. This is roughly what Figures A17 & A18 show for the effective metallicity at the half-light radius versus $M_{H_m,K}$ and V_{rot} (central values are too uncertain due to likely higher concentrations of dust and seeing mismatches, and PB00's models do not consider bulges). Unfortunately, our galaxies do not exceed $V_{\rm rot} \sim 250$ km s⁻¹, but the general trend above, including the decrease in scatter with $V_{\rm rot}$, is confirmed.

The right side of Figure A24 shows our measured metallicity gradients as a function of total galaxy magnitude; gradients in disk scale lengths are shown in the upper panels while gradients in kpc are shown underneath. The left and right panels show the "inner" and "outer" gradients respectively. When plotted against scale length, the inner or outer gradients show no clear trends. However, when plotted in kpc, a trend emerges such that brighter galaxies have smaller gradients. Since scale length increases with luminosity (see Fig. A1), the correlation goes away when the gradients are measured per disk scale length. If this effect is real, the disappearance of a trend of metallicity gradients in units of scale length may suggest a self-similar pattern in disk

galaxies. As suggested by Combes (1998), a "universal" slope per disk scale length might be explained by the viscous disk models of Lin & Pringle (1987), although model predictions are not conclusive as of yet. The Garnett et al. (1997) compilation of O/H gradients shows a similar signature, where abundance gradients in dex/kpc are steeper and exhibit greater scatter for lower luminosity disks, but this trend goes away when gradients are expressed in dex/h. Note, however, that the abundance gradients compiled in van Zee et al. (1998) and reported in PB00 do show a clear increase with magnitude when plotted as dex/h, thus thwarting the interpretation of a universal abundance gradient per scale length.

We have measured compelling trends for the effective age and metallicity in spiral galaxies and their inner and outer disk gradients as a function of surface brightness, luminosity, rotational velocity, and size. These trends are not well reproduced by current semi-analytical models of galaxy evolution but will undoubtedly serve as effective constraints for future models. An important limitation inherent in our color-based analysis is its sensitivity to dust extinction which could mimic gradients in age and, particularly, metallicity. A spectroscopic analysis of radially resolved line indices of spiral galaxies is underway in order to alleviate this problem.

APPENDIX

HILINE WIDTHS

H I line widths were collected from various sources in the literature; Courteau (1997) [7gals]; Bottinelli et al. (1990) [74 gals]; Theureau et al. (1998) [11 gals]; Haynes et al. (1999) [1 gal]; de Blok & Bosma (2002) [1 gal]; de Blok, McGaugh, & Rubin (2001) [4 gals]. For the Bottinelli et al. (1990) and Theureau et al. (1998) samples, the line width at 20% and 50% of the peak flux, W50 and W20, were provided, though not for all galaxies. In cases where only W20 was available, a conversion to W50 was made from a linear least-squares fit between these two quantities derived from those for galaxies for which both measurements were available. The conversions between the fully corrected line widths are as follows:

For the Bottinelli et al. (1990) sample: W50 = 0.98 * W20 - 19.21 [N = 3325]For the Theureau et al. (1998) sample: W50 = 1.00 * W20 - 17.01 [N = 2055]

Haynes et al. (1999) give a different measure of the line width denoted W21 and defined as the full width between the velocity channels at the 50% level of each horn. We can convert the Haynes et al. (1999)'s W21 to Bottinelli et al. (1990)'s W50 as: W50(Bot) = 1.02 * W21(Haynes) + 1.39 [N = 275],

and Courteau (1997)'s $V_{\rm max}$ and Botinelli et al. (1990)'s W50 are matched with:

 $W50(Bot) = 0.99 * V_{\text{max}} - 9.31 [N = 122]$

For 4 of the LSBs in the BdJ00 sample we obtained V_{max} values from de Blok, McGaugh, & Rubin (2001) and de Blok & Bosma (2002). A comparison between the Courteau (1997) V_{max} values and the Bottinelli et al. (1990) W50s for galaxies in common reveals little difference, and we assume here that V_{max} values for the LSBs also map directly into W50.

Multiple measurements of a galaxy from different samples vary typically by less than 10%, more than accurate enough for our purposes. In order to ensure accurate V_{rot} measurements, we restricted ourselves to galaxies with inclinations greater than 35°. Our final sample has 98 galaxies with reliable rotational velocity measurements.

REFERENCES

Abraham, R. G., Ellis, R. S., Fabian, A. C., Tanvir, N. R., & Glazebrook, K. 1999, MNRAS, 303, 641
Balcells, M., Graham, A. W., Domínguez-Palmero, L., & Peletier, R. F. 2003, ApJ, 582, L79
Bell, E. F., McIntosh, D. H., Katz, N., & Weinberg, M. D. 2003, ApJS, in press, astro-ph/0302543
Bell, E. F. & Bower, R. G. 2000, MNRAS, 319, 235
Bell, E. F. & de Jong, R. S. 2000, MNRAS, 312, 497

Bell, E. F. & de Jong, R. S. 2001, ApJ, 550, 212
Bica, E., Alloin, D., & Schmidt, A. 1990, MNRAS, 242, 241
Bottinelli, L., Gouguenheim, L., Fouque, P., & Paturel, G. 1990, A&AS, 82, 391

Bruzual, G. & Charlot, S. 2003, MNRAS, in press, astro-ph/0309134

Burstein, D. 1979, ApJ, 234, 435

Burstein, D. & Heiles, C. 1984, ApJS, 54, 33

Byun, Y. I. & Freeman, K. C. 1995, ApJ, 448, 563

Byun, Y. I., Freeman, K. C., & Kylafis, N. D. 1994, ApJ, 432, 114 Carlberg, R. G. 1984, ApJ, 286, 403

Chabrier, G. 2003, PASP, 115, 763

Charlot, S. & Silk, J. 1994, ApJ, 432, 453

Cole, S., Lacey, C. G., Baugh, C. M., & Frenk, C. S. 2000, MNRAS, 319, 168

Courteau, S. 1996, ASSL Vol. 209: New Extragalactic Perspectives in the New South Africa, 255

Courteau, S., de Jong, R. S., & Broeils, A. H. 1996, ApJ, 457, L73 Courteau, S. & van den Bergh, S. 1999, AJ, 118, 337

Courteau, S., MacArthur, L. A., Dekel, A., van den Bosch, F., McIntosh, D. H., & Dale, D. 2004, ApJ, submitted Dalcanton, J. J. & Bernstein, R. A. 2002, AJ, 124, 1328de Blok, W. J. G. & Bosma, A. 2002, A&A, 385, 816

de Blok, W. J. G., McGaugh, S. S., & Rubin, V. C. 2001, AJ, 122, 2396

de Jong, R. S. 1996, A&AS, 118, 557

Disney, M., Davies, J., & Phillipps, S. 1989, MNRAS, 239, 939
Emsellem, E. et al. 2002, ASP Conf. Ser. 282: Galaxies: the Third Dimension, 189

Evans, R. 1994, MNRAS, 266, 511

Falco, E. E. et al. 1999, PASP, 111, 438

Fioc, M. & Rocca-Volmerange, B. 1997, A&A, 326, 950

Freeman, K. & Bland-Hawthorn, J. 2002, ARA&A, 40, 487

Garnett, D. R., Shields, G. A., Skillman, E. D., Sagan, S. P., & Dufour, R. J. 1997, ApJ, 489, 63

Garnett, D. R. 2002, astro-ph/0211148

Garnett, D. R. 2002a, ApJ, 581, 1019

Gavazzi, G., Bonfanti, C., Sanvito, G., Boselli, A., & Scodeggio, M. 2002, ApJ, 576, 135

Gordon, K. D., Calzetti, D., & Witt, A. N. 1997, ApJ, 487, 625 Guarnieri, M. D., Dixon, R. I., & Longmore, A. J. 1991, PASP

Guarnieri, M. D., Dixon, R. I., & Longmore, A. J. 1991, PASP, 103, 675

Haynes, M. P. & Giovanelli, R. 1984, AJ, 89, 758

Haynes, M. P., Giovanelli, R., Chamaraux, P., da Costa, L. N., Freudling, W., Salzer, J. J., & Wegner, G. 1999, AJ, 117, 2039

Holmberg, E. 1946, Medd. Lund. Astron. Obs., Ser II, No. 117
Jarrett, T. H., Chester, T., Cutri, R., Schneider, S. E., & Huchra,
J. P. 2003, AJ, 125, 5

Kauffmann, G. 1996, MNRAS, 281, 487

Kauffmann, G. et al. 2003, MNRAS, 341, 33

Kauffmann, G. et al. 2003, MNRAS, 341, 54

Kroupa, P. 2002, Science 295, 82

Kuchinski, L. E., Terndrup, D. M., Gordon, K. D., & Witt, A. N. 1998, AJ, 115, 1438

Landolt, A. U. 1992, AJ, 104, 340

Larson, R. B. 1974, MNRAS, 166, 585

MacArthur, L. A., Courteau, S., & Holtzman, J. A. 2003, ApJ, 582, 689

Maraston, C. 2003, astro-ph/0301419

Martin, C. L. 2003, The IGM/Galaxy Connection: The Distribution of Baryons at z=0, ASSL Conference Proceedings Vol. 281. Edited by J. L. Rosenberg & M. E. Putman. ISBN: 1-4020-1289-6, Kluwer Academic Publishers, Dordrecht, 2003

Martin, P. & Roy, J. 1994, ApJ, 424, 599

Masters, K. L., Giovanelli, R., & Haynes, M. 2003, ApJ, in press. astro-ph/0304398

Matteucci, F. 2002, Chemical Evolution of Galaxies and Intracluster Medium, Proceedings of the XII Canary Islands Winter School of Astrophysics, on "Cosmochemistry: the melting pot of elements"., November 19th-30th 2001, Tenerife, Spain astro-ph/0203340

Matthews, L. D. & Wood, K. 2001, ApJ, 548, 150

Mehlert, D., Thomas, D., Saglia, R. P., Bender, R, & Wegner, G. 2003, A&A, in press. astro-ph/0306219

Meurer, G. R. 2000, ASP Conf. Ser. 211: Massive Stellar Clusters, 81

Mo, H. J., Mao, S., & White, S. D. M. 1998, MNRAS, 295, 319Möllenhoff, C. & Heidt, J. 2001, A&A, 368, 16

Nilson, P. 1973, Nova Acta Regiae Soc. Sci. Upsaliensis Ser. V Peletier, R. F., Valentijn, E. A., Moorwood, A. F. M., Freudling, W., Knapen, J. H., & Beckman, J. E. 1995, A&A, 300, L1

Peletier, R. F., Balcells, M., Davies, R. L., Andredakis, Y., Vazdekis, A., Burkert, A., & Prada, F. 1999, MNRAS, 310, 703 Prantzos, N. & Boissier, S. 2000, MNRAS, 313, 338

Salpeter, E. E. 1955, ApJ, 121, 161

Sandage, A. 1986, A&A, 161, 89

Schiavon, R. P., Faber, S. M., Castilho, B. V., & Rose, J. A. 2002, ApJ, 580, 850

Searle, L., Sargent, W. L. W., & Bagnuolo, W. G. 1973, ApJ, 179, 427

Sellwood, J. A. & Binney, J. J. 2002, MNRAS, 336, 785 Somerville, R. S. & Primack, J. R. 1999, MNRAS, 310, 1087 Spergel, D.N. et al. (2003) astro-ph/0302209

Theureau, G., Bottinelli, L., Coudreau-Durand, N., Gouguenheim, L., Hallet, N., Loulergue, M., Paturel, G., & Teerikorpi, P. 1998, A&AS, 130, 333

Tinsley, B. M. & Gunn, J. E. 1976, ApJ, 203, 52

Tully, R. B. & Verheijen, M. A. W. 1997, ApJ, 484, 145

Valentijn, E. A. 1990, Nature, 346, 153

Witt, A. N., Thronson, H. A., & Capuano, J. M. 1992, ApJ, 393, 611

Wyse, R. F. G. 1999, The Formation of Galactic Bulges, 195 Xilouris, E. M., Byun, Y. I., Kylafis, N. D., Paleologou, E. V., & Papamastorakis, J. 1999, A&A, 344, 868

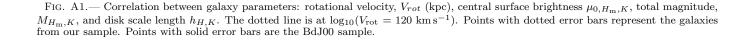


Fig. A2.— Correlation between galaxy parameters and morphological type. The dotted line is at $\log_{10}(V_{\rm rot}=120~{\rm km\,s^{-1}})$.

Fig. A3.— Comparison of the stellar population model tracks for different initial mass functions; the Salpeter (1955) IMF (eq. 2), and the Chabrier (2003) IMF (eq. 4) for the GALAXEV models (left panel) and of the Salpeter versus the Kroupa (2001) (eq. 3) IMFs for the PEGASE models (right panel). The GALAXEV models are also plotted on the right panel for comparison between two different SSP models.

Fig. A4.— Time evolution for the exponential (eq. 6), upper panel, and Sandage (eq. 8), lower panel, star formation histories (solid curves). The dotted curve is a Sandage-style burst of star formation in which 10% of the total mass of stars are formed. See Figure A7 for the effect of such a burst on the population model grids.

Fig. A5.— Comparison of the stellar population model tracks for exponential (eq. 6) and Sandage (eq. 8) star formation histories.

Fig. As.— Depression after a stripe to the control of the stripe and the control of the stripe and the control of the stripe and the stripe a (action) than strates that the state H the state H constant H c the Courteau et al. sample, converted to K-band with 2MASS H-K colors (see text for details) for direct comparison with the K-band data of the BdJ00 sample.

Fig. A7.— Comparison of the stellar population model tracks for a simple exponential SFH (eq. 6) and one with a 4 Gyr old Sandage

(eq. 8) burst contributing 10% of the total mass (left plot, and see Figure A4) and 50% of the mass (right plot). Fig. A9.— Near-IR-optical color-color plots for the Courteau et al. sample separated by morphological type. The galaxy centers are indicated by solid symbols: circles for Type-I galaxies, triangles for Type-II, and asterisks for Transition galaxies. Open circles denote the half-light radius of the disk. The line types for the galaxy color profiles represent bar strength: solid for bar-less (A), dashed for mild bars (AB), and dot-dashed for strong bars (B). Average errors due to the global calibration, as well as sky uncertainties for the innermost and outermost points are shown as crosses. Over-plotted are the Bruzual & Charlot (2003; GALAXEV) stellar population models for an exponential SFH at different metallicities. Lines of constant average age $\langle A \rangle$ (see eq.10) are the dashed, roughly vertical lines, while lines of constant metallicity are solid and nearly horizontal. In the upper left corner of each panel, triplex and foreground screen dust models are plotted. For the triplex model, the Milky Way dust extinction curve and albedo from Gordon, Calzetti, & Witt (1997) was adopted. The galaxy center and disk half-light radius are denoted by solid and open circles respectively.

Fig. A10.— Near-IR–optical color–color plots for the Courteau et al. sample separated by rotational velocity, $V_{\rm rot}~({\rm km\,s^{-1}})$. Symbols and line-types are as in Figure A9.

 $\label{eq:Fig.A11.} \textbf{Fig. A11.} \textbf{--} \textbf{Near-IR-optical color-color plots separated by rotational velocity}, \textit{V}_{\text{rot}} \ (\text{km}\,\text{s}^{-1}), \text{ for the BdJ00 sample.}$

Fig. A12.— Near-IR—optical color—color plots for the Courteau et al. sample separated by H-band magnitude, M_H . Symbols and line-types are as in Figure A9.

Fig. A13.— Near-IR–optical color–color plots for the Courteau et al. sample separated by H-band central surface brightness, $\mu_{0,H}$. Symbols and line-types are as in Figure A9.

Fig. A14.— Average age, $\langle A \rangle$ (left), and metallicity, $\log_{10}(Z/Z_{\odot})$ (right) as a function of local $H_{\rm m}$ and K-band surface brightness, where $H_{\rm m}$ is the "modified" H-band SB for the Courteau et al. sample, converted to K-band with 2MASS H-K colors (see text for details) for direct comparison with the K-band data of the BdJ00 sample. The $H_{\rm m}$ data is distinguished with dotted error bar lines. The different symbols represent total $H_{\rm m}, K$ -band magnitude bins for each galaxy. The dotted lines in the metallicity plot (right) denote the limits of the population model grids. Points at or near these limits for metallicity, and those at 12.9 Gyr for the average age should be interpreted with caution.

Fig. A15.— "Effective" average age (average of 0.5–1.5h bin), $\langle A \rangle_{\rm eff}$ as a function of central surface brightness (left) and total H_m , K-band galaxy magnitude (right) for all 158 galaxies. See caption of Figure A14 for the definition of H_m .

Fig. A16.— "Effective" average age as a function of scale length (left) for all 158 galaxies and rotational velocity (right), $V_{\rm rot}$ for all 98 galaxies for which we have reliable $V_{\rm rot}$ measurements.

Fig. A17.— "Effective" metallicity $\log_{10}(Z_{\rm eff}/Z_{\odot})$ as a function of central surface brightness (left) and total $H_{\rm m}, K$ -band galaxy magnitude (right) for all 158 galaxies. See caption of Figure A14 for the definition of $H_{\rm m}$.

Fig. A18.— "Effective" metallicity, $\log_{10}(Z_{\rm eff}/Z_{\odot})$, as a function of scale length (left) for all 158 fitted galaxies, and rotational velocity (right), $V_{\rm rot}$ for all 98 galaxies for which we have reliable $V_{\rm rot}$ measurements.

Fig. A19.— Age as a function of radius for all galaxies. The left plot gives the radius in terms of the measure scale length $h_{H,K}$ while the right plot gives the radius in physical units (kpc). Dotted lines represent our sample whereas solid lines are the BdJ00 sample.

Fig. A20.— Same as Figure A19 but for metallicity.

Fig. A21.— Age gradient as a function of central surface brightness, $\mu_{0,H_{\mathrm{m}},K}$ for all galaxies. The gradients are fit out to a different number of radial bins: 0–1.5 $h_{H,K}$ (top left), 0–2.5 $h_{H,K}$ (top right), 0–3.5 $h_{H,K}$ (bottom left), and 0–4.5 $h_{H,K}$ (bottom right).

Fig. A22.— Age gradient as a function of $H_{\rm m}$,K-band central surface brightness, $\mu_{0,H_{\rm m},K}$ (left) and total magnitude, $M_{H_{\rm m},K}$ (right) for all galaxies. The fit ranges represent "inner" gradients (left panels) fit out to 1.5 H,K-band disk scale lengths, $h_{H,K}$, and "outer" gradients (right panels) fit from 1.5 to 3.5 $h_{H,K}$. The upper and lower plots show gradients as a function of scale length and kpc respectively.

 $\mbox{Fig. A23.} \mbox{---} \mbox{Same as Figure A22 except for disk scale lengths, } \log(h_{H,K}) \mbox{ (left), and rotational velocity, } V_{\rm rot} \mbox{ (right)}.$

Fig. A24.— Same as Figure A22 except for metallicity gradients.

Fig. A26.— Metallicity gradient as a function of age gradient for all 158 galaxies.

Fig. A27.— Effective age (left) and metallicity (right) as a function of morphological type for all 158 galaxies.

Fig. A25.— Same as Figure A23 except for metallicity gradients.

Fig. A28.— Age gradient (left) and metallicity gradient (right) as a function of morphological type for all 158 galaxies. The upper panels plot radius in terms of the measured scale length $h_{H,K}$ while the bottom panels plot radius in physical units (kpc).

Fig. A29.— Age gradient (left) and metallicity gradient (right) histograms as a function of barredness for all 158 galaxies. The upper panels plot the radius in terms of the measured scale length $h_{H,K}$ while the bottom panels plot the radius in physical units (kpc). The fit ranges represent "inner" gradients (left panels) fit out to 1.5 $h_{H,K}$, and "outer" gradients (right panels) fit from 1.5 to 3.5 $h_{H,K}$. The vertical dotted lines are located at zero gradient for reference.